THE JOURNAL OF PHYSICAL CHEMISTRY C

Article

Cite This: J. Phys. Chem. C 2018, 122, 3363−3370

pubs.acs.org/JPCC

TiO_2(B) and Anatase Angstrom-Scale Wires: A Theoretical Study

Luciana Fernández-Werner,*[,†] Estela A. González,[‡] Ricardo Faccio,*[,†] and Álvaro W. Mombrú[†]

[†]Centro NanoMat/CryssMat-Lab, DETEMA, Facultad de Química, Universidad de la República, Montevideo, Uruguay

[‡]Instituto de Física del Sur (IFISUR), Departamento de Física, Universidad Nacional del Sur (UNS), CONICET, Av. L. N. Alem 1253, B8000CPB - Bahía Blanca, Argentina

Supporting Information

ABSTRACT: In this work, we model TiO_2(B) angstrom-scale wires derived from TiO_2(B) (001) ultrathin sheets. By means of density functional theory (DFT) calculations, we study their structural, electronic and thermodynamic properties, comparing with anatase angstrom scale wire with *z* as growing direction, of which there is experimental evidence. We found locally stable structures. TiO_2(B) atomic wire oriented along *y* direction exhibits significantly lower formation energy (0.33 eV) than the other studied systems (1.05 eV for TiO_2(B) wire oriented along *x*- and 0.88 eV for anatase wire oriented along *z*-direction). Additionally, we present the simulated X-ray powder diffraction diagrams in order to help the experimental identification of this potential titanium dioxide polymorph's nanostructures. These results could be interesting for their potential applications, such as energy storage and photovoltaic applications, and for fundamental studies as well.

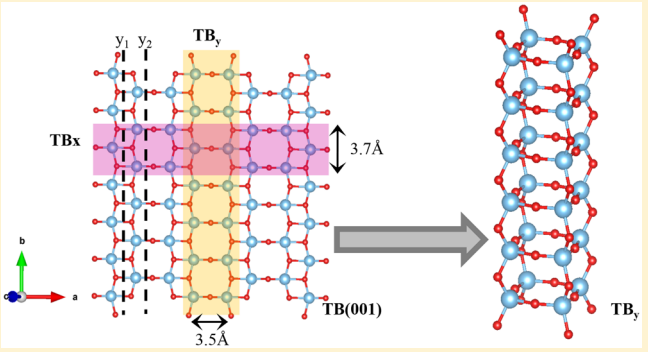

1. INTRODUCTION

One-dimensional (1D) TiO_2 nanostructures have received much attention due to their unique properties. High aspect ratio, large specific surface area, chemical stability, and excellent electronic properties allow their use in photocatalysis, sensors, solar cells, hydrogen production and storage, lithium-ion batteries, and biomedicine. The synthesis, structure, properties, and applications have been reviewed previously in the literature.[1−4]

Reaching the maximum of miniaturization, bulk synthesis of extremely thin crystalline anatase TiO_2 atomic wires with diameters of a few angstroms (∼4 to 5 Å) and growth direction [001] was reported some years ago by Liu and Yang.[5] Using a chemical solution method, they obtained nearly monodisperse wires, with N-doping on the surfaces and capped by a protective surface layer of oleic acid. Then, Iacomino et al. performed first-principle calculations on anatase nanowires investigating structural and electronic properties dependence on the size, growth direction and surface coverage with hydrogen and water.[6]

These one-dimensional systems are very promising for fundamental study of physical and chemical properties at the nanoscale. In particular, due to the small radius and the fact that most of the atoms are on the surfaces, quantum and surface effects are projected to be more relevant, which leads to important changes in physical and chemical properties. From a technological point of view, it could be used as building blocks in devices engineering as well.

On the other hand, at the nanoscale, the interest in polymorph B of titanium dioxide (TiO_2(B)) is growing, since it appears as a metastable phase during thermal annealing of low contain sodium layered titanate nanostructures obtained via alkali hydrothermal synthesis.[7] Additionally, the theoretically observation of an exceptional low energy formation of ultrathin TB(001) slab has been reported.[8,9] It is important to mention that TB(001) presents normalized formation energy of 0.38 J m^{-2}, and the other cutting surfaces such as TB(100) presents a considerably higher normalized formation energies of 0.83 J m^{-2}.

According to these results, the aim of this work is to theoretically generate atomic wires derived from TiO_2(B) polymorph, particularly from the (001) surface, and to study its structural, electronic, and thermodynamic properties in comparison to another well-known atomic scale wires, such as anatase atomic wires.

2. METHODOLOGY

2.1. System Selection. Atomic wires named TB_x and TB_y are obtained by fragmentation of TB(001) ultrathin sheet according to Figure 1 where [100] and [010] are respectively growth directions. In all the cases we kept the stoichiometry in order to ensure a 1:2 Ti:O ratio. As previously shown,[8,10] the bilayer named TB(001) goes into a reconstruction where atoms reach a very symmetrical configuration. All the titanium atoms present a square pyramidal geometrical environment, which

Received: October 23, 2017
Revised: January 23, 2018
Published: January 24, 2018

DOI: 10.1021/acs.jpcc.7b10418
J. Phys. Chem. C 2018, 122, 3363−3370

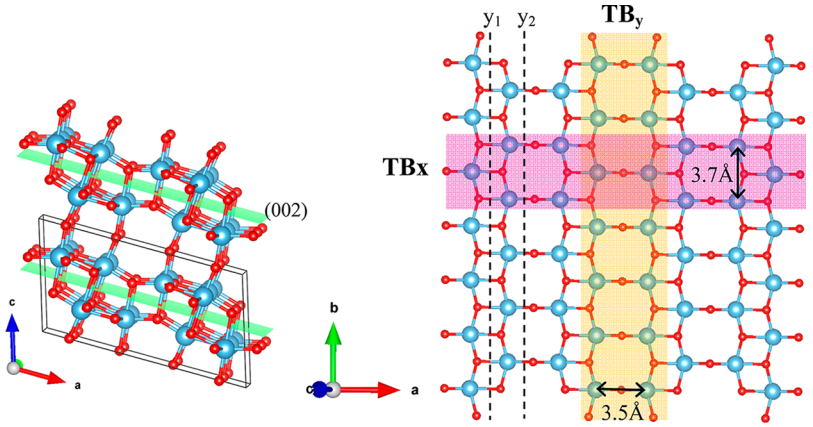

Figure 1. (a) Scheme of the obtaining of TB(001) bilayer and (b) TB angstrom-scale wires starting from TB(001) ultrathin sheet.

appears to act stabilizing the structure. Because of this, in the case of TB_y, we select the bonds to cut analogously as when obtaining TB(001) bilayer from the bulk. In the case of TB(001) cutting plane was (002) as shown in Figure 1, and in the case of TB_y we cut along y_1 plane shown in the same figure. The TB_y atomic wire obtained this way is also very symmetric having all the titanium atoms tetrahedral environments. In the case of TB_x, due to the structural symmetry of TB(001), the cutting options were equivalent when considering similar wire thickness than A_z model (according to experimental evidence ~3.8 Å[5]).

Conversely, we decided to work with an anatase atomic wire along [001] (named A_z, Figure 2), in accordance with

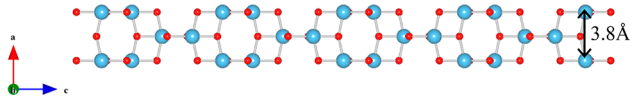

Figure 2. Initial structure of A_z atomic wire.

experimental reports that was mentioned before.[5] In the three cases, we performed calculations periodically along axis direction. All the models and figures were prepared with VESTA.[11]

2.2. Computational Details. All the wires were simulated using *ab initio* methods by utilizing density functional theory (DFT).[12,13] For the calculations, VASP (Vienna ab initio Simulation Package),[14−17] with the GGA (generalized gradient approximations) exchange-correlation functional with the PBE parametrization (Perdew−Burke−Ernzerhof) was utilized.[18,19] Projected augmented wave method (PAW)[20] used GGA-PBE potentials with the following valence electrons: Ti ($3s^2$ $3p^6$ $4s^2$ $3d^2$) and O ($2s^2$ $2p^4$). A *k*-space grid of 1 × 1 × 21 points was used, utilizing 21 points in the periodic direction and 1 × 1 in the vacuum directions. The cutoff energy for the plane wave expansion was selected as 500 eV. Additionally, we performed a further single point calculation, using the hybrid xc-functional HSE06,[21] in order to get a better description of the electronic structure, particularly for the description of the energy band gaps.

The structures were optimized until reaching a force tolerance in all the atoms of 0.005 eV/Å. The unit cell was optimized, following the stress tensor until reaching a tolerance of the diagonal components of 0.25 kBar.

After the first structural optimization, we performed a vibrational analysis by means of density functional perturbation theory (DFPT),[22−25] as implemented in VASP and utilizing the Phonopy[26] code for the post processing. With the phonon's dispersion diagram, we look for the imaginary branch, in order to force a further structural optimization, following the involved eigenvectors, with the purpose to obtain and confirm the local minima for all the described atomic scale wires. Here it is important to mention that we included long-range interactions for the macroscopic electric field induced by polarization of eigenvectors close to the Γ-point. The nonanalytical term (NAC) is included in the dynamical matrix $D_{\alpha\beta}$ as follows:[27−29]

$$D_{\alpha\beta}(jj', \vec{q} \to 0) = D_{\alpha\beta}(jj', \vec{q} = 0) + \frac{1}{\sqrt{m_i m_j}} \frac{4\pi}{\Omega_0} \frac{\left(\sum_\gamma q_\gamma Z^*_{j,\gamma\alpha}\right)\left(\sum_{\gamma'} q_{\gamma'} Z^*_{j',\gamma'\beta}\right)}{\sum_{\alpha\beta} q_\alpha \varepsilon^\infty_{\alpha\beta} q_\beta} \quad \text{(i)}$$

where α and β are the Cartesian indices; j and j' are the indices of atoms in a unit cell; l, l' are the indices of unit cell; $Z^*_{j,\gamma\alpha}$ represents de Born effective charge tensor of the j atom in the cell, and $\varepsilon^\infty_{\alpha\beta}$ is the high frequency static dielectric tensor. The correction to frequencies at the rest of q-points are interpolated according to the methodology reported by Wang et al.[30] With this procedure it is possible to introduce the dipole−dipole interactions, that describes the LO−TO splitting for these polar materials.

Finally, Helmholtz vibrational free energy (F_{vib}) according to eq ii, harmonic vibrational energy (E_{vib}) according to eq iii, vibrational entropy (S_{vib}) according to eq iv and heat capacity at constant volume (C_V) according to eq v,were obtained from the phonon dispersion. We reported all the previously mentioned properties in the range of T = 0 to 1000 K.

$$F_{vib} = E_{vib} - TS_{vib} \quad \text{(ii)}$$

$$E_{vib} = \sum_{q\nu} \hbar\omega(q\nu)\left[\frac{1}{2} + \frac{1}{e^{\hbar\omega(q\nu)/k_B T} - 1}\right] \quad \text{(iii)}$$

DOI: 10.1021/acs.jpcc.7b10418
J. Phys. Chem. C 2018, 122, 3363−3370

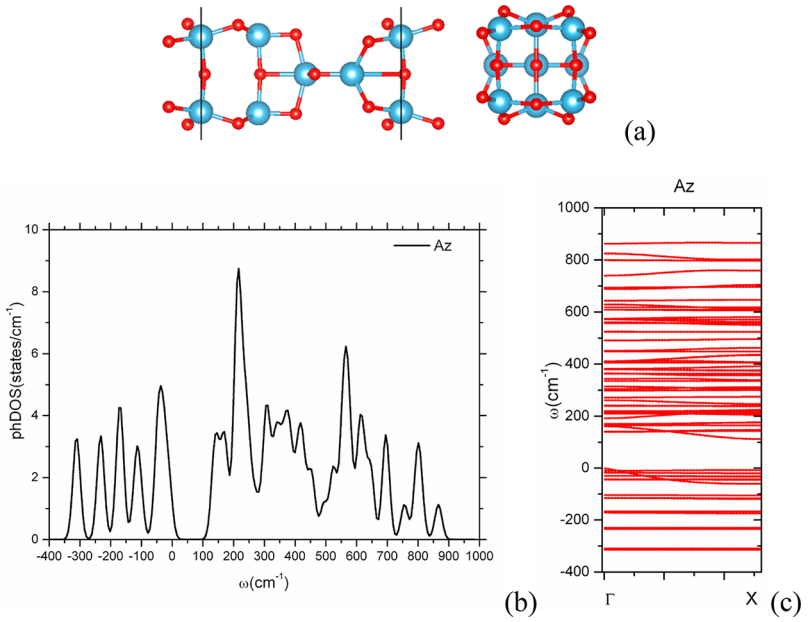

Figure 3. (a) Schematic view of anatase (001) wire and (b) the corresponding phonon dispersion with (c) density of phononic states.

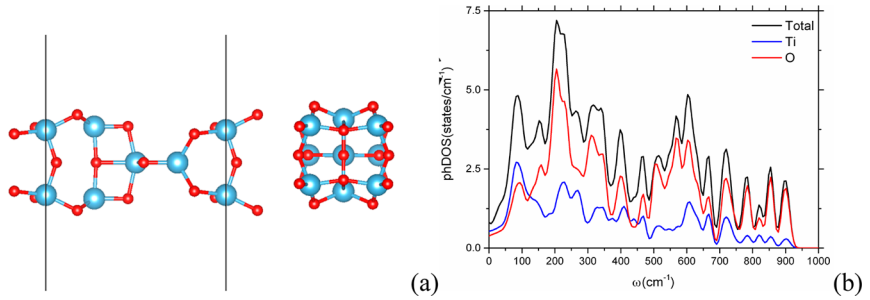

Figure 4. (a) Schematic view of anatase (001) wire modulated-Γ and (b) its corresponding phonon dispersion with density of phononic states.

$$S_{vib} = -\frac{\partial F_{vib}}{\partial T} = \frac{1}{2T}\sum_{q\nu}\hbar\omega(q\nu)\coth(e^{\hbar\omega(q\nu)/2k_BT}) - k_B\sum_{q\nu}\ln\left[2\sinh\left(\frac{\hbar\omega(q\nu)}{2k_BT}\right)\right] \quad \text{(iv)}$$

$$C_V = \left(\frac{\partial E}{\partial T}\right)_V = \sum_{q\nu}k_B\left(\frac{\hbar\omega(q\nu)}{k_BT}\right)^2\left\{\frac{e^{\hbar\omega(q\nu)/k_BT}}{(e^{\hbar\omega(q\nu)/k_BT}-1)^2}\right\} \quad \text{(v)}$$

2.3. X-ray Powder Diffraction (XRPD) and *g*(*r*) Simulations. After obtaining the atomic wires optimized structures, we proceed with the simulation of the diffraction patterns with the Debye method through Debyer software[31] and pair distribution functions $g(r)$ using the OVITO open visualization tool.[32] The aim of these calculations was to shed some light on structural rearrangements.

3. RESULTS AND DISCUSSION

3.1. Geometry Optimization. *Anatase Atomic Wire (A_z).* After the conventional structural optimization, we proceed with the phonon analysis, that revealed 22 branches with imaginary frequencies in their respectively phonon dispersion, as it is shown in Figure 3. Inspecting the phonon dispersion, it is clear that major instability occurs for modes projected eigenvectors to the Γ-point. Consequently, following atomic displacements corresponding to these eigenvectors it is possible to reach more rapidly the local minimum, which was not possible to obtain after the conventional structural optimization. For that reason, we studied the effect of the structural modulation in the original anatase structure. Figure 4 shows new phononic density of states and phonons dispersion corresponding now to modulated structure after reoptimization. For the modulation at the Γ-point, the original unit-cell was selected due to the fact that all the displacements, related to all the eigenvectors, remain commensurate inside the original unit cell.

Modulated structure was submitted to structural optimization. Phonons calculation reveals, in this case, only three imaginary frequencies modes, which we attribute to corresponding acoustic branches of the structure.

After the wire creation, the original geometry of bulk anatase become distorted, as it is evident when computing simulated DRX pattern as well as pair distribution function (Figure 5)

The variation in the periodic parameter *c* is not significant (~0.2%), from 9.51 Å in case of bulk anatase[33] to 9.49 Å in A_z wire. The structural distortion is more notorious in the alternated Ti−O square parallel to the plane ***ab***. An inward contraction is observed along the ***b*** direction where distance d_3 between oxygen atoms changes from 3.71 Å (before modulation) to 2.64 Å. In agreement to this contraction corresponding titanium atoms distance d_5 changes from 3.45 to

DOI: 10.1021/acs.jpcc.7b10418
J. Phys. Chem. C 2018, 122, 3363−3370

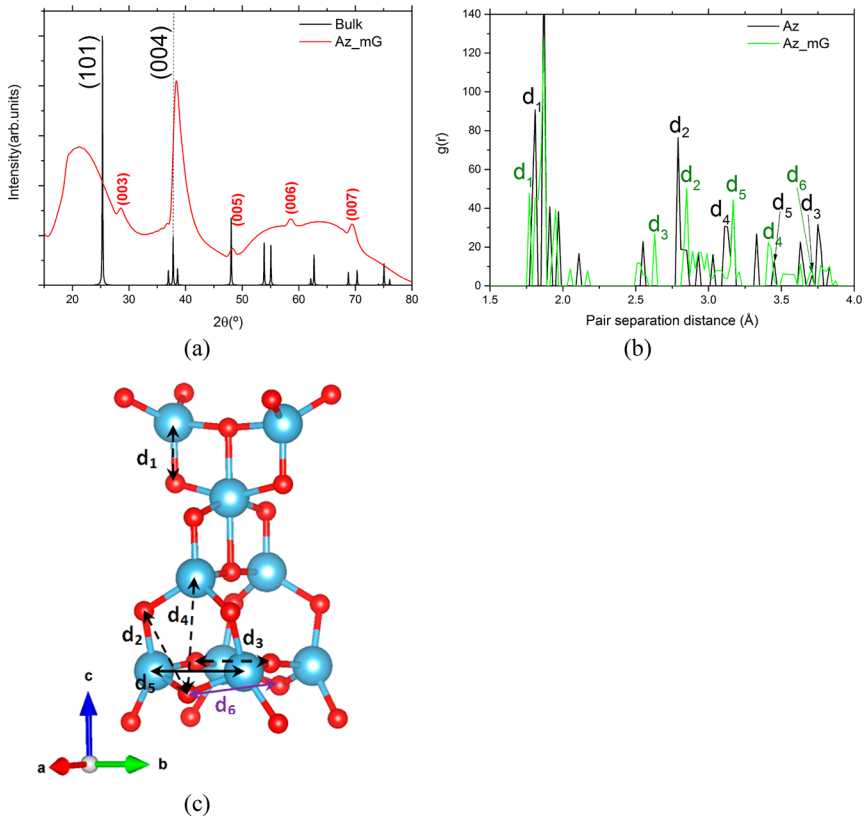

Figure 5. (a) Simulated XR diffraction pattern considering 10 nm length atomic wire in comparison with bulk pattern. (b) Pair distribution function $g(r)$ corresponding to A_z atomic wire before (A_z) and after (A_z_mG) optimization (mG comes from modulation at the Γ-point) (c) Unit cell of A_z after optimization showing the distances called on $g(r)$.

3.17 Å. In contrast, an outward expansion is observed along ***a*** direction where d_6 changes from 3.71 to 4.79 Å. Change in distances between corresponding titanium atoms is less significant (3.44 Å to 3.58 Å).

Regarding DRX pattern, a sharp peak is observed at 2θ = 38.4° which corresponds with an interplanar distance of 2.37 Å in agreement with (004) bulk reflection evidencing the growth direction of the wire. Coherent signals corresponding to distances c/3, c/5, c/6, and c/7 (fractions of the periodic parameter c) due to the lowering of crystal symmetry are evident although with lower intensity (C_{2v} ($mm2$) in case of A_z wire). Bulk anatase exhibits a tetragonal system with symmetry according to the space group $I4_1/amd$, where the reflections (003), (005), (006), and (007) are not allowed.

The broad bump located near $2\theta \sim 20°$ is associated with the bulk anatase (101) reflection. The broadness is coherent with the fact that atomic wires are extremely thin, and the shift to smaller angles reflects the expansion found in ***a*** that, since axial parameter remains constant, causes an expansion of the (101) interlayer distance. This is not evident in reported experimental data due to the low statistics of diffraction pattern.[5] However, final distances between the two pairs of outermost Ti atoms are in excellent agreement with previously reported theoretically calculations by Iacomino et al.[6] In their work, they found distances between the two outermost Ti atoms along [100] of 3.1467 Å and a distance between the two outermost Ti atoms along [010] of 3.566 Å; in this work, we found 3.17 and 3.58 Å, respectively.

TB_x and TB_y Atomic Wires. In the case of both atomic wires derived from B polymorph, imaginary frequencies can be attributed to acoustics branches (Figure 6 and Figure 7). Thus, we consider these structures as locally stable.

Both TB wires show a contraction of periodic parameters comparing with initial values, being more notoriously in the

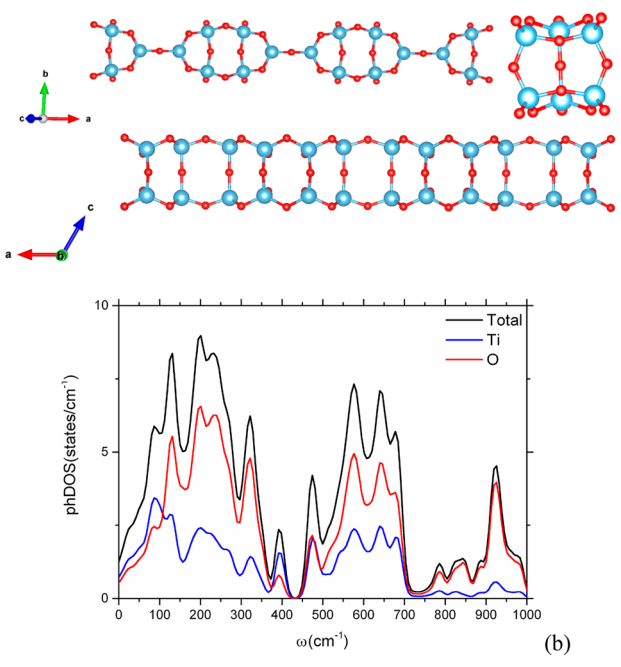

Figure 6. Schematic view of TB_x atomic wire and its corresponding phonon dispersion diagram with density of phononic states.

DOI: 10.1021/acs.jpcc.7b10418
J. Phys. Chem. C 2018, 122, 3363−3370

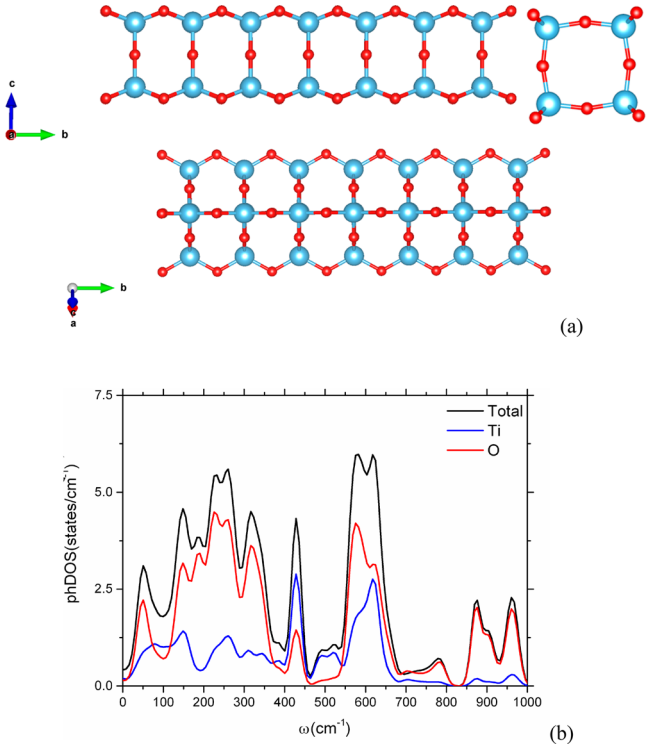

Figure 7. (a) Schematic view of TB_y atomic wire and (b) the corresponding phonon dispersion with density of phononic states.

case of TB_y from 3.74 to3.23 Å (13.6%).This reflects the change of titanium atoms coordination, which changes from square pyramidal to tetrahedral environment. For TB_x this change is from 12.18 to 11.73 Å, which represents a 3.7% variation.

TiO_2(B) is a monoclinic system with space group C_2/m. The diffraction pattern of TB_x shows a principal sharp peak corresponding to (400) reflection which is coherent with axial direction ([100]). It also evidence a loss of symmetry where appear peaks associated with crystallographic planes (h00), perpendicular to axial direction, with $h \neq 2n$ (Figure 8).

On the other hand, TB_y notoriously presents higher order symmetry, presenting point group $D_{4h}(4/mmm)$ with a structural tolerance of 0.1 Å. In this case, DRX defined peaks correspond to (020) and (040) reflections according to the growth direction (cell parameter b). Pair distribution function of TB_x (Figure 8f) also evidence this higher symmetry, showing less and more defined peaks.

3.2. Energetic and Electronic Properties. The comparison of formation energies per unit of TiO_2 are listed in Table 1 and were determined using expression vi, where E_{wire} stands for the total energy of the atomic-wire, $E_{TiO2\text{-}bulk}$ is the total energy of the corresponding bulk structure, and N_{Ti} corresponds to the number of TiO_2 units inside the wire and corresponding bulk structure, respectively.

$$E_{form}(eV) = \frac{E_{wire}}{N_{Tiwire}} - \frac{E_{TiO_2bulk}}{N_{Tibulk}} \quad \text{(vi)}$$

All the atomic wires present positive formation energies, as expected, where $TB_y < A_z < TB_x$. These results are in principle expected, since the amount of under-coordinated atoms in these atomic wires are very high when compared with other wider wires or wider surface slabs of TiO_2. Nevertheless, A_z and TB_x presents similar formation energies, but TB_y presents a considerable lower formation energy, less than a half. These results could be expressed in terms of the gained symmetry in the case of TB_y in comparison to TB_x, as observed in the final geometries and also evidenced in the simulated diffraction patterns.

Furthermore, in both TB models, after optimization, all the titanium atoms have tetrahedral environment. However, in TB_x [TiO4] tetrahedra have higher degree of distortion which is evident when comparing O−Ti−O angles. In the case of TB_y the mean value is 109.3° and standard deviation is 5.7° while in TB_x the mean angle is 108.9° and the standard deviation 8.7°. Considering that the ideal angle of a tetrahedral coordination is 109.5°, TB_y mean angle is closest and the dispersion is lowest (Figure S.I.2, Supporting Information). Another way to compare the distortion is by considering the Ti−O bond length distortion index, denoted DI(TO), as described by Baur,[34] eq vii, which expresses the average deviation of Ti−O bond length. TO_i and TO_m stand for the individual and the mean distances from titanium to oxygen atoms, respectively. Mean DI(TO) values are 0.0063 and 0.0074 for TB_y and TB_x respectively which reinforce that the tetrahedral distortion is higher in TB_x model consistent with stabilization of TB_y in comparison to TB_x.

$$\mathrm{DI(TO)} = \sum_{i=1}^{4} \frac{|\mathrm{TO}_i - \mathrm{TO}_m|}{4\mathrm{TO}_m} \quad \text{(vii)}$$

The results are promising, since experimentally[5] it was argued that a system similar to A_z was obtained, and according to our calculations it could be possible to prepare and obtain similar TB atomic wires. While the relative formation energies are still somehow high, a further stabilization could be gained protecting the surface of the wires, e.g., utilizing small surfactant molecules or utilizing different solvents.

In reference to the band gap energies, there is an increase in the values when compared to the bulks ones, as expected and mainly due to the generated quantum confinement. With the purpose to report the energy as precise as possible, we utilized GGA-PBE and HSE06 as xc-functionals in order to limit the values, using a functional that underestimates and overestimates the band gap, respectively (see Table 1).

In the case of PBE, the E_{gap} follows the trend $E_{gap\_A_z} < E_{gap\_TB_x} < E_{gap\_TB_y}$, but when HSE06 is chosen, all the energy gaps become equivalents to ∼4.25 eV. For these reason, we would expect in general a relatively similar energy gap for all the described atomic scale wires. Figure 9 presents the electronic density of states, analogously to bulk TiO_2 polymorphs, the valence band is composed of p-states mainly contributed from oxygen atoms, while conduction band mostly contributed from the d-states of titanium atoms.

3.3. Thermodynamic Properties. Having the phonon dispersion, it is easy to evaluate the main thermodynamic properties such as entropy (S), Helmholtz free energy (F) and internal energy (E). In the case of solids, the influence of the pressure could be minimized, and thus the internal energy corresponds to the enthalpy (H); and the Helmholtz free energy (F) approximates to the Gibbs free energy (G).[35] In particular, for the case of Gibbs free energy we included the ground state electronic total energy in order to compare G for all the wires and polymorphs: $\boldsymbol{G(V, T) \cong E_{wire}(V) - F_{vib}(V, T)}$.

DOI: 10.1021/acs.jpcc.7b10418
J. Phys. Chem. C 2018, 122, 3363−3370

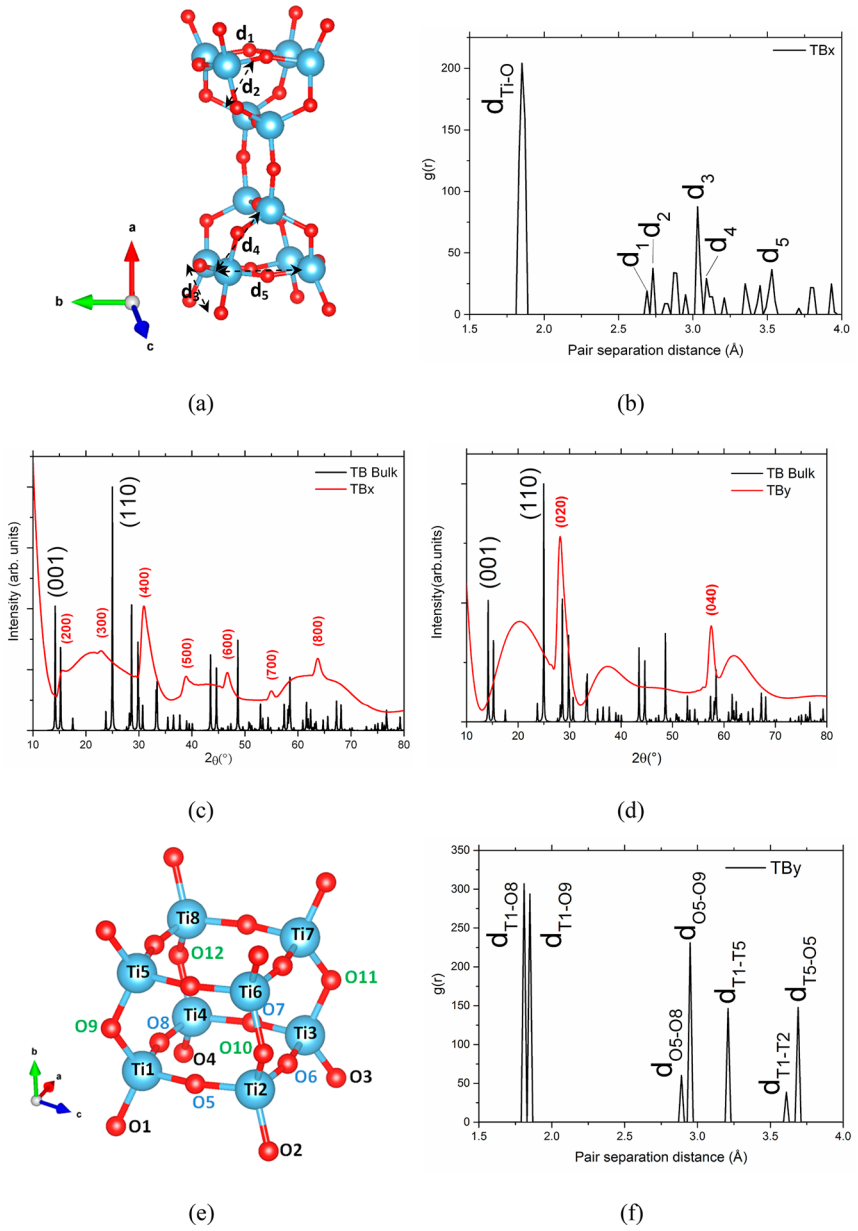

Figure 8. (a) Optimized building block of TB_x, (b) pair distribution function g(r) corresponding to TB_x after optimization, (c) simulated XR diffraction pattern considering 10 nm length TB_x atomic wire in comparison with bulk TiO_2(B) pattern, (d) simulated XR diffraction pattern considering 10 nm length TB_y atomic wire in comparison with bulk TiO_2(B) pattern, (e) optimized building block of TB_y showing the distances called on $g(r)$, and (f) pair distribution function $g(r)$ corresponding to TB_y atomic wire after optimization.

Table 1. Formation Energies per Unit of TiO_2 and Energy Gaps Calculated with GGA-PBE and HSE06

system	N_{Tiwire}	chemical formula	E_{form} (eV)	$E_{gap\ PBE}$ (eV)	$E_{gap\ HSE06}$ (eV)	$E_{gap\ bulk\ PBE}$ (eV)	$E_{gap\ bulk\ HSE06}$ (eV)
TB_x	36	$Ti_{12}O_{24}$	1.05	3.19	4.30	2.73	4.33
TB_y	12	Ti_4O_8	0.33	3.62	4.25	2.73	4.33
A_z	27	Ti_9O_{18}	0.88	2.71	4.21	2.23	3.70

As can be observed in Figure 10, the relative stability favors the TB_y wire in comparison to A_z and final TB_x, for a very wide range of temperature from 0 to 1000 K, and in concordance to formation energies early reported. The reason for that behavior is the similar contribution from the vibrational energy and entropy from all the studied wires, as observed in the early presented phonon density of states, being the electronic energy the main contribution from the observed differences. In the case of C_v, in the low temperature regime $T < 250$ K there are no important differences, the changes occur for $T > 250$ K, where it is observed the following trend: $C_{v\_TB_x} > C_{v\_A_z} > C_{v\_TB_y}$. Finally, and with the purpose to indirectly evaluate the bond strength in the atomic wires, the Debye temperature Θ_D was estimated. It is well-known that there is no a unique way to estimate Θ_D; for this reason, we just selected one method and then we performed a comparative study between the atomic wires and the corresponding bulk structures. Utilizing the

DOI: 10.1021/acs.jpcc.7b10418
J. Phys. Chem. C 2018, 122, 3363−3370

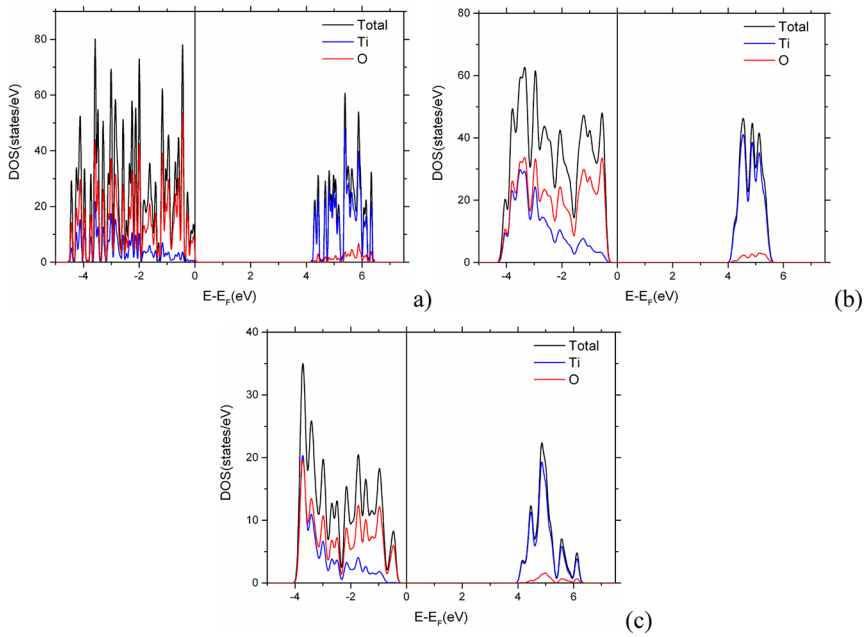

Figure 9. Electronic density of states for (a) A_z, (b) TB_x, and (c) TB_y, utilizing HSE06 as the xc-functional.

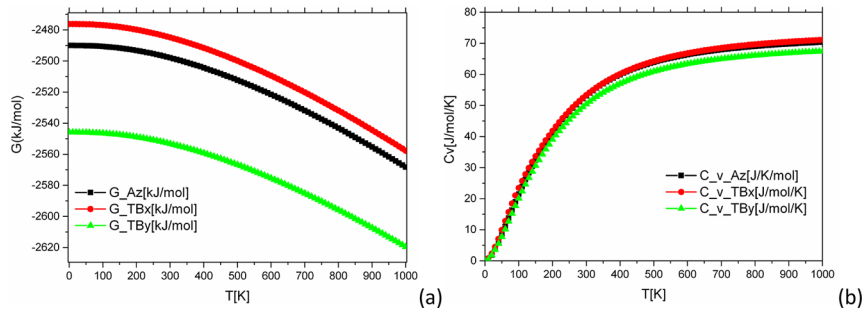

Figure 10. (a)Gibbs free energy and (b) C_v for: A_z, TB_x, and TB_y.

phonon density of states (phDOS), and performing a $a\omega^2$ fitting, up to $^1/_4$ of the frequency range, it was possible to obtain the following values for Θ_D: 706, 702, and 698 K for A_z, TB_x, and TB_y, respectively. It allows us to conclude that the relative bond strength is higher for A_z in comparison to the TB wires, although the differences are not very pronounced. However, when compared to the corresponding values for bulk anatase and TiO_2(B) the obtained values correspond to Θ_D = 688 and 656 K respectively. According to these results, the formation of the atomic wires induces relatively hardening of the Ti−O bonds.

4. CONCLUSIONS

In this work, we optimized the structure of bare atomic wires derived from TiO_2(B) (001) ultrathin sheet and anatase, finding locally stable structures. There is one in particular, TB_y, which has significantly lower formation energy in comparison to the rest of the studied atomic wires. All these structures were characterized in terms of structural, electronic, and thermodynamic properties.

■ ASSOCIATED CONTENT

Supporting Information

The Supporting Information is available free of charge on the ACS Publications website at DOI: 10.1021/acs.jpcc.7b10418.

New images of the wire models, O−Ti−O angle distribution, and atomic coordinates (PDF)

■ AUTHOR INFORMATION

Corresponding Authors

*E-mail: rfaccio@fq.edu.uy.
*E-mail: lucianaf@fq.edu.uy.

ORCID

Luciana Fernández-Werner: 0000-0002-8119-2467
Ricardo Faccio: 0000-0003-1650-7677

Notes

The authors declare no competing financial interest.

■ ACKNOWLEDGMENTS

The authors wish to thank the Uruguayan funding institutions CSIC (CSIC 710−I+D 2011), ANII and PEDECIBA. E.A.G. is a member of CONICET. We acknowledge financial support from SGCyT-UNS, ANPCyT-PICT 2014-1351, and CONICET-PIP 2014-2016 GI 11220130100436CO.

■ REFERENCES

(1) Wang, X.; Li, Z.; Shi, J.; Yu, Y. One-Dimensional Titanium Dioxide Nanomaterials: Nanowires, Nanorods, and Nanobelts. *Chem. Rev.* **2014**, *114*, 9346−9384.

DOI: 10.1021/acs.jpcc.7b10418
J. Phys. Chem. C 2018, 122, 3363−3370

(2) Tian, J.; Zhao, Z.; Kumar, A.; Boughton, R. I.; Liu, H. Recent Progress in Design, Synthesis, and Applications of One-Dimensional Tio2 Nanostructured Surface Heterostructures: A Review. *Chem. Soc. Rev.* **2014**, *43*, 6920−6937.
(3) Ge, M.; Cao, C.; Huang, J.; Li, S.; Chen, Z.; Zhang, K.-Q.; Al-Deyab, S.; Lai, Y. A Review of One-Dimensional Tio 2 Nanostructured Materials for Environmental and Energy Applications. *J. Mater. Chem. A* **2016**, *4*, 6772−6801.
(4) Zhou, W.; Liu, H.; Boughton, R. I.; Du, G.; Lin, J.; Wang, J.; Liu, D. One-Dimensional Single-Crystalline Ti-O Based Nanostructures: Properties, Synthesis, Modifications and Applications. *J. Mater. Chem.* **2010**, *20*, 5993−6008.
(5) Liu, C.; Yang, S. Synthesis of Angstrom-Scale Anatase Titania Atomic Wires. *ACS Nano* **2009**, *3*, 1025−1031.
(6) Iacomino, A.; Cantele, G.; Trani, F.; Ninno, D. Dft Study on Anatase Tio2 Nanowires: Structure and Electronic Properties as Functions of Size, Surface Termination, and Morphology. *J. Phys. Chem. C* **2010**, *114*, 12389−12400.
(7) Morgado, E.; de Abreu, M. A.; Pravia, O. R.; Marinkovic, B. A.; Jardim, P. M.; Rizzo, F. C.; Araújo, A. S. A Study on the Structure and Thermal Stability of Titanate Nanotubes as a Function of Sodium Content. *Solid State Sci.* **2006**, *8*, 888−900.
(8) Vittadini, A.; Casarin, M.; Selloni, A. Structure and Stability of Tio2-B Surfaces: A Density Functional Study. *J. Phys. Chem. C* **2009**, *113*, 18973−18977.
(9) Fernández-Werner, L.; Faccio, R.; Juan, A.; Pardo, H.; Montenegro, B.; Mombrú, Á. W. Ultrathin (001) and (100) Tio 2 (B) Sheets: Surface Reactivity and Structural Properties. *Appl. Surf. Sci.* **2014**, *290*, 180−187.
(10) Vittadini, A.; Casarin, M. Ab Initio Modeling of Tio 2 Nanosheets. *Theor. Chem. Acc.* **2008**, *120*, 551−556.
(11) Momma, K.; Izumi, F. Vesta 3 for Three-Dimensional Visualization of Crystal, Volumetric and Morphology Data. *J. Appl. Crystallogr.* **2011**, *44*, 1272−1276.
(12) Hohenberg, P.; Kohn, W. Inhomogeneous Electron Gas. *Phys. Rev.* **1964**, *136*, B864−B871.
(13) Kohn, W.; Sham, L. J. Self-Consistent Equations Including Exchange and Correlation Effects. *Phys. Rev.* **1965**, *140*, A1133−A1138.
(14) Kresse, G.; Hafner, J. Ab Initio Molecular Dynamics for Liquid Metals. *Phys. Rev. B: Condens. Matter Mater. Phys.* **1993**, *47*, 558−561.
(15) Kresse, G.; Hafner, J. Ab Initio Molecular-Dynamics Simulation of the Liquid-Metal-Amorphous-Semiconductor Transition in Germanium. *Phys. Rev. B: Condens. Matter Mater. Phys.* **1994**, *49*, 14251−14269.
(16) Kresse, G.; Furthmüller, J. Efficient Iterative Schemes for Ab Initio Total-Energy Calculations Using a Plane-Wave Basis Set. *Phys. Rev. B: Condens. Matter Mater. Phys.* **1996**, *54*, 11169−11186.
(17) Kresse, G.; Furthmüller, J. Efficiency of Ab-Initio Total Energy Calculations for Metals and Semiconductors Using a Plane-Wave Basis Set. *Comput. Mater. Sci.* **1996**, *6*, 15−50.
(18) Perdew, J. P.; Burke, K.; Ernzerhof, M. Generalized Gradient Approximation Made Simple. *Phys. Rev. Lett.* **1996**, *77*, 3865−3868.
(19) Perdew, J. P.; Burke, K.; Ernzerhof, M. Generalized Gradient Approximation Made Simple [Phys. Rev. Lett. 77, 3865 (1996)]. *Phys. Rev. Lett.* **1997**, *78*, 1396−1396.
(20) Blöchl, P. E. Projector Augmented-Wave Method. *Phys. Rev. B: Condens. Matter Mater. Phys.* **1994**, *50*, 17953−17979.
(21) Krukau, A. V.; Vydrov, O. A.; Izmaylov, A. F.; Scuseria, G. E. Influence of the Exchange Screening Parameter on the Performance of Screened Hybrid Functionals. *J. Chem. Phys.* **2006**, *125*, 224106.
(22) Baroni, S.; Giannozzi, P.; Testa, A. Green's-Function Approach to Linear Response in Solids. *Phys. Rev. Lett.* **1987**, *58*, 1861−1864.
(23) Gonze, X. Perturbation Expansion of Variational Principles at Arbitrary Order. *Phys. Rev. A: At., Mol., Opt. Phys.* **1995**, *52*, 1086−1095.
(24) Gonze, X. Adiabatic Density-Functional Perturbation Theory. *Phys. Rev. A: At., Mol., Opt. Phys.* **1995**, *52*, 1096−1114.
(25) Baroni, S.; de Gironcoli, S.; Dal Corso, A.; Giannozzi, P. Phonons and Related Crystal Properties from Density-Functional Perturbation Theory. *Rev. Mod. Phys.* **2001**, *73*, 515−562.
(26) Togo, A.; Tanaka, I. First Principles Phonon Calculations in Materials Science. *Scr. Mater.* **2015**, *108*, 1−5.
(27) Giannozzi, P.; de Gironcoli, S.; Pavone, P.; Baroni, S. Ab Initio. *Phys. Rev. B: Condens. Matter Mater. Phys.* **1991**, *43*, 7231−7242.
(28) Gonze, X.; Lee, C. Dynamical Matrices, Born Effective Charges, Dielectric Permittivity Tensors, and Interatomic Force Constants from Density-Functional Perturbation Theory. *Phys. Rev. B: Condens. Matter Mater. Phys.* **1997**, *55*, 10355−10368.
(29) Pick, R. M.; Cohen, M. H.; Martin, R. M. Microscopic Theory of Force Constants in the Adiabatic Approximation. *Phys. Rev. B* **1970**, *1*, 910−920.
(30) Wang, Y.; Wang, J. J.; Wang, W. Y.; Mei, Z. G.; Shang, S. L.; Chen, L. Q.; Liu, Z. K. A Mixed-Space Approach to First-Principles Calculations of Phonon Frequencies for Polar Materials. *J. Phys.: Condens. Matter* **2010**, *22*, 202201.
(31) Debyer https://github.com/wojdyr/debyer.
(32) Stukowski, A. Visualization and Analysis of Atomistic Simulation Data with Ovito−the Open Visualization Tool. *Modell. Simul. Mater. Sci. Eng.* **2010**, *18*, 015012.
(33) Horn, M.; et al. Refinement of the Structure of Anatase at Several Temperatures*. *Zeitschrift für Kristallographie* **1972**, *136*, 273.
(34) Baur, W. H. The Geometry of Polyhedral Distortions. Predictive Relationships for the Phosphate Group. *Acta Crystallogr., Sect. B: Struct. Crystallogr. Cryst. Chem.* **1974**, *B30*, 1195−1215.
(35) Mei, Z.-G.; Wang, Y.; Shang, S.-L.; Liu, Z.-K. First-Principles Study of Lattice Dynamics and Thermodynamics of Tio2 Polymorphs. *Inorg. Chem.* **2011**, *50*, 6996−7003.

DOI: 10.1021/acs.jpcc.7b10418
J. Phys. Chem. C 2018, 122, 3363−3370